JACS
JOURNAL OF THE AMERICAN CHEMICAL SOCIETY

Communication

pubs.acs.org/JACS

Gold Quantum Boxes: On the Periodicities and the Quantum Confinement in the Au_{28}, Au_{36}, Au_{44}, and Au_{52} Magic Series

Chenjie Zeng,[†] Yuxiang Chen,[†] Kenji Iida,[‡,∥] Katsuyuki Nobusada,*[,‡,∥] Kristin Kirschbaum,[§] Kelly J. Lambright,[§] and Rongchao Jin*[,†]

[†]Department of Chemistry, Carnegie Mellon University, Pittsburgh, Pennsylvania 15213, United States

[‡]Department of Theoretical and Computational Molecular Science, Institute for Molecular Science, Myodaiji, Okazaki 444-8585, Japan

[∥]Elements Strategy Initiative for Catalysts and Batteries (ESICB), Kyoto University, Katsura, Kyoto 615-8520, Japan

[§]Department of Chemistry and Biochemistry, University of Toledo, Toledo, Ohio 43606, United States

Supporting Information

ABSTRACT: Revealing the size-dependent periodicities (including formula, growth pattern, and property evolution) is an important task in metal nanocluster research. However, investigation on this major issue has been complicated, as the size change is often accompanied by a structural change. Herein, with the successful determination of the $Au_{44}(TBBT)_{28}$ structure, where TBBT = 4-*tert*-butylbenzenethiolate, the missing size in the family of $Au_{28}(TBBT)_{20}$, $Au_{36}(TBBT)_{24}$, and $Au_{52}(TBBT)_{32}$ nanoclusters is filled, and a neat "magic series" with a unified formula of $Au_{8n+4}(TBBT)_{4n+8}$ (n = 3−6) is identified. Such a periodicity in magic numbers is a reflection of the uniform anisotropic growth patterns in this magic series, and the n value is correlated with the number of (001) layers in the face-centered cubic lattice. The size-dependent quantum confinement nature of this magic series is further understood by empirical scaling law, classical "particle in a box" model, and the density functional theory calculations.

Magic-sized metal nanoclusters are often regarded as an analogue to atoms, with the metal atoms in the nanocluster mimicking the nucleons in the atom and the free valence electrons resembling the electrons in the atom.[1−6] Such an analogue between the different-scale objects provides an intuitive way to understand the unknown system. Then an interesting question arises: Will the nanoclusters exhibit the same periodicity as atoms in the periodic table? Recent advances in thiolate-protected gold nanoclusters (denoted as $Au_n(SR)_m$) have led to the discovery of a number of magic sizes, and their structural construction rules have been partially understood.[7] However, most of the magic sizes were obtained by changing the surface-protecting thiolates, which resulted in largely varied structures.[8−12] It is still unclear whether there are periodic series of nanoclusters, or they are completely random, i.e., every size comes as a surprise.

The study of the property evolution of metal nanoclusters is also complicated by the interference from variations in the surface ligands and the types of structures (e.g., face-centered cubic (fcc) vs icosahedron vs decahedron).[7,9−14] It is known that when the size of gold nanoclusters is smaller than 2−3 nm, their optical properties become dominated by quantum confinement effects.[1,15−18] However, the optical gaps of the $Au_n(SR)_m$ nanoclusters exhibit zigzag behavior with increasing size, albeit the overall trend is that the gap gradually closes up.[7] This is unlike other quantum systems with the same structural types, such as the semiconductor quantum dots or conjugated alkenes, in which a monotonic decreasing of band gap is observed with increasing size.[19] Thus, in order to explore the growth pattern and property evolution rules, it is highly desirable to obtain a series of magic sizes with no complications by different structural types and different surface ligands.

Herein, we report the discovery of periodicities in gold nanoclusters protected by the same 4-*tert*-butyl-benzenethiolate (TBBT). This "magic series" includes $Au_{28}(TBBT)_{20}$, $Au_{36}(TBBT)_{24}$, $Au_{44}(TBBT)_{28}$, and $Au_{52}(TBBT)_{32}$. The "magic" nature of this series is reflected in the general formula of $Au_{8n+4}(SR)_{4n+8}$, with n = 3−6. Such a neat progression of magic number is shown in the mass spectra of the four nanoclusters (Figure 1). A uniform spacing of m/z 2237 is identified, corresponding to $Au_8(TBBT)_4$. In previous work, we studied the structures of Au_{28}, Au_{36}, and Au_{52},[20] with a "hole" in Au_{44}. Here,

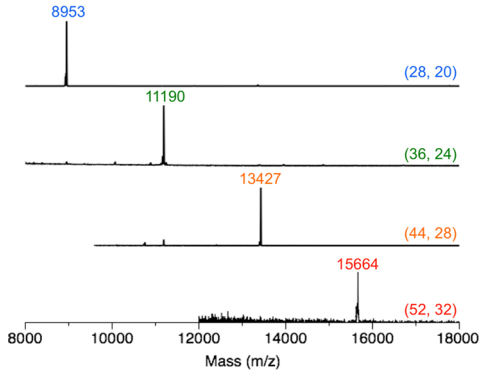

Figure 1. Electronspray ionization mass spectra (ESI-MS) of the magic series nanoclusters. The m/z = $[Au_n(TBBT)_m + Cs]^+$.

Received: December 6, 2015
Published: March 2, 2016

DOI: 10.1021/jacs.5b12747
J. Am. Chem. Soc. 2016, 138, 3950−3953

we have succeeded in structure determination of the missing link—the $Au_{44}(TBBT)_{28}$ nanocluster (see Supporting Information for details), which finally completes the "magic series". The growth patterns and size-dependent properties in this "magic series" can now be unambiguously examined.

The gold atoms in the $Au_n(SR)_m$ nanoclusters can be divided into two categories: those in the kernel and those in the surface $Au_x(SR)_{x+1}$ staple motifs. However, the boundary between the kernel and surface gold atoms is not explicit in some cases (e.g., the fcc nanoclusters).[20c] Below, we provide three alternative views of the structures of the magic series, as well as the corresponding growth patterns, based on the analysis of the Au−Au bond lengths. Figure S1 shows four steps of increasing bond lengths in $Au_{44}(TBBT)_{28}$, similar to others in the series.[20c]

In the first view, gold atoms with the shortest Au−Au bond length are considered as the kernel atoms (Figure S1, stage I). The kernel structural unit in this view is made up by two helixes of tetrahedra (Figure 2A). The gold kernel grows by successively adding two tetrahedra to the bottom of the double helixes, resulting in 4 tetrahedra in $Au_{28}(TBBT)_{20}$, 6 tetrahedra in $Au_{36}(TBBT)_{24}$, 8 tetrahedra in $Au_{44}(TBBT)_{28}$, and 10 tetrahedra in $Au_{52}(TBBT)_{32}$ (Figure 2A). The two ends of the double helixes are protected by $Au_2(SR)_3$ dimeric staples (Figure 2B, in yellow), whereas the waists are protected by different staples depending on the length of double helixes, with $Au_3(SR)_4$ trimers for Au_{28}, dimers for Au_{36}, and dimers plus $Au(SR)_2$ monomers for Au_{44} and Au_{52}. This is the most divided view, since each gold atom connected to two sulfur atoms is dissected from the kernel and viewed as a surface atom. Previous theoretical studies used this anatomy to understand the structures,[21−23] and the segregation of tetrahedron units was also observed by X-ray spectroscopy.[24] In addition, the electronic configuration of the magic series nanoclusters can be explained to some extent by the tetrahedron-based model.[20c] In the progression from $Au_{28}(TBBT)_{20}$, $Au_{36}(TBBT)_{24}$, $Au_{44}(TBBT)_{28}$, to $Au_{52}(TBBT)_{32}$, the formal electron count increases from 8e, 12e, 16e, to 20e, which matches with the 4, 6, 8, and 10 tetrahedral units in the nanoclusters, with each tetrahedral unit requiring two electrons for stabilization.

For the second view, more gold atoms are included into the kernel since these gold atoms are also quite closely connected to the kernel (Figure S1, stage III). It gives rise to a structural view based on interpenetrating cuboctahedra. As shown in Figure 2C, the nanocluster grows through sequential interpenetration of additional two cuboctahedral units at the bottom of the smaller kernel. Thus, as the nanocluster grows from $Au_{28}(TBBT)_{20}$, $Au_{36}(TBBT)_{24}$, $Au_{44}(TBBT)_{28}$, to $Au_{52}(TBBT)_{32}$, the kernels evolve from two-, four-, six-, to eight-interpenetrating cuboctahedra. During the growth, the total number of Au_5 or Au_6 {111} facets remains at four (Figure 2D, green shade), while the total number of Au_4 {100} squares increases from 8, 12, 16, to 20 (Figure 2D, magenta shade). The surface-protecting modes obey the same rules, i.e., each {111} facet is protected by one dimeric staple (Figure 2E, green lines), and each {100} square is protected by one bridging thiolate (Figure 2E, yellow balls). Such an interpenetrating-cuboctahedron view was applied to explain the structures of Au_{28} and Au_{36}[20a,b] and to predict the structure of Au_{44},[25] and recently applied to the Au_{52}.[26] It is also reminiscent of "cluster of clusters" or the polyhedron-fusion mode in the growth of phosphine-protected Au/Ag alloy as well as palladium nanoclusters.[27]

The growth pattern in the magic series can be further simplified into a concise layer-by-layer mode (Figure 2F,G).

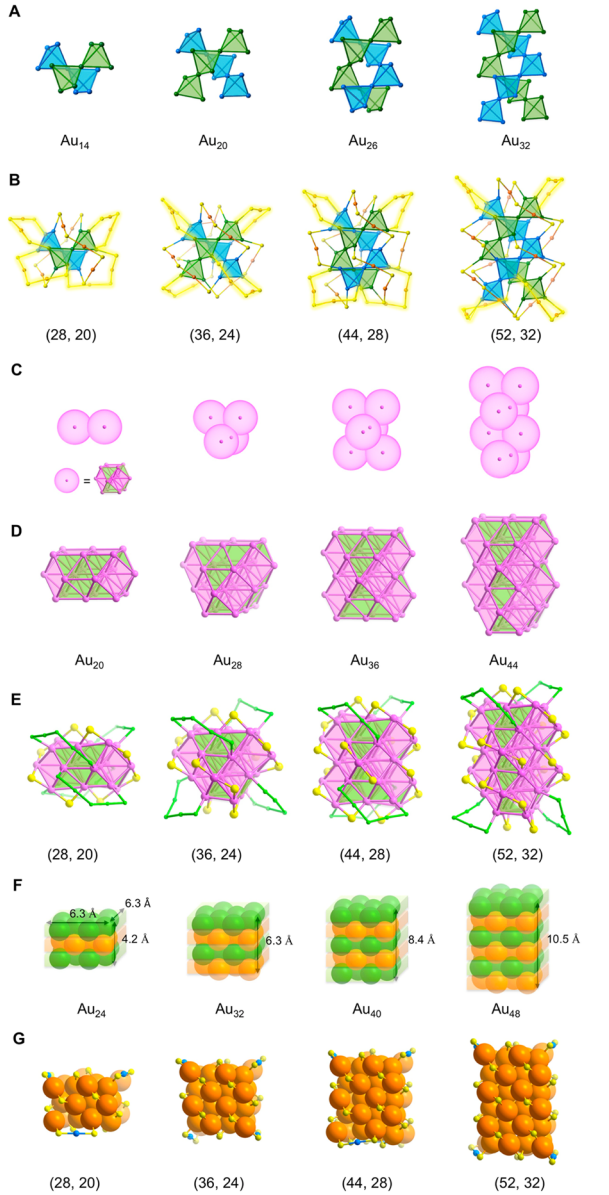

Figure 2. Three views of the growth patterns in the $Au_{8n+4}(SR)_{4n+8}$ magic series, n = 3−6: (A,B) Tetrahedron coiling up; (C−E) cuboctahedron interpenetration; (F,G) anisotropic growth of the fcc lattice. Yellow = S, others = Au, green line = S−Au−S−Au−S.

When incorporating four more gold atoms into the kernel of each nanocluster, the kernel evolves into a regular fcc-based "box", with all six surfaces being exclusively terminated by {100} facets. The growth of the kernel is achieved through subsequently adding an additional eight gold-atom (001) layer along the z-direction, with the x- and y-directions being constant. Thus, there are three, four, five, and six (001) layers of Au_8 in the $Au_{28}(TBBT)_{20}$, $Au_{36}(TBBT)_{24}$, $Au_{44}(TBBT)_{28}$, and $Au_{52}(TBBT)_{32}$, which corresponds to n = 3−6 in $Au_{8n+4}(TBBT)_{4n+8}$, respectively (Figure 2F). As to the gold−thiolate interface structure, the magic series nanoclusters all share the same rules, i.e., pairs of gold atoms on the {100} facets are anchored by simple bridge thiolates, while the left-out gold atoms at the top and the bottom edges are anchored by four additional monomeric staples (Figure 2G, blue balls for Au atoms in the monomers). Such a growth pattern is reminiscent of the growth of nanoparticles into one-dimensional (1D) nanorods[28a] and

DOI: 10.1021/jacs.5b12747
J. Am. Chem. Soc. 2016, 138, 3950−3953

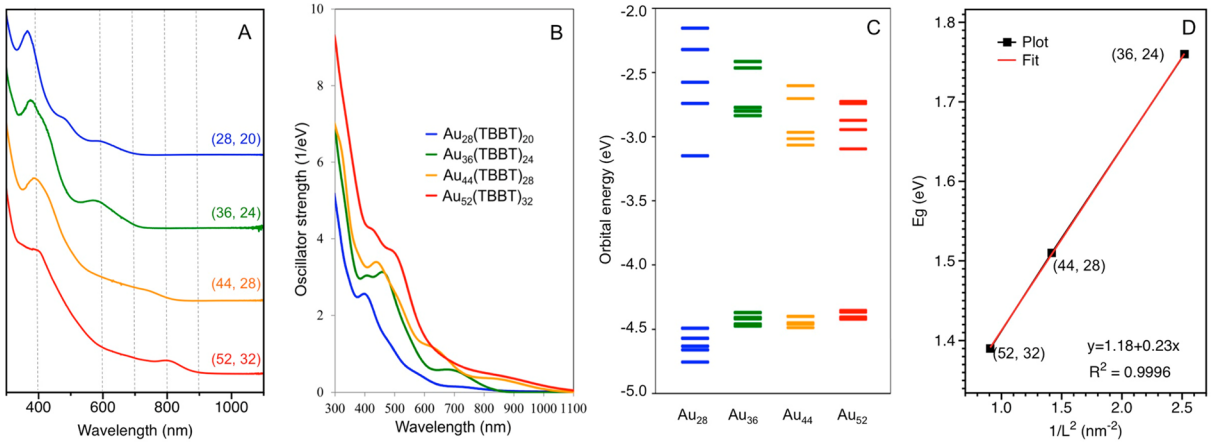

Figure 3. Quantum confinement nature in the $Au_{8n+4}(TBBT)_{4n+8}$ magic series. (A) size-dependent UV–vis spectra; DFT-calculated (B) oscillator strengths and (C) energy levels (HOMO−4 to LUMO+4); and (D) scaling law of energy gap with size.

provides atomic-scale insight into the anisotropic growth of nanoparticles.[20c]

Naturally, a question is whether the uniform growth patterns can be further extended. Theoretically, this magic series can be expanded to n = 7−10, ... (i.e., 7-layered $Au_{60}(TBBT)_{36}$, 8-layered $Au_{68}(TBBT)_{40}$, 9-layered $Au_{76}(TBBT)_{44}$, and 10-layered $Au_{84}(TBBT)_{48}$, ..., respectively). This will eventually lead to elongated fcc nanorods, with a fixed diameter. The further elongated $Au_{8n+4}(TBBT)_{4n+8}$ ($n > 6$) may possibly be synthesized via careful adjusting of the reduction kinetics. Recently, Takano et al.[28b] reported a kinetically controlled synthesis of $Au_{76}(SR)_{44}$, and its structure was believed to be a fcc rod but with a different structure from what we discussed above. Toward the smaller end of the $Au_{8n+4}(TBBT)_{4n+8}$ series, $n = 2$ gives rise to $Au_{20}(TBBT)_{16}$; its structure has been crystallographically characterized[29] and follows the tetrahedron growth pattern as reflected in its vertex-sharing Au_7 bitetrahedral kernel, but this structure does not fit into the other two patterns (Figure 2D and 2F). Further reducing the size, i.e., $n = 1$, leads to $Au_{12}(TBBT)_{12}$, which would only have one atomic layer, and it indeed evolves into a complex with two $Au_6(TBBT)_6$ rings (i.e., a catenane structure),[30] and no Au(0) atoms exists in $Au_{12}(TBBT)_{12}$.

It is worth mentioning that, except the $Au_{36}(TBBT)_{24}$, all the other nanoclusters in the $Au_{8n+4}(TBBT)_{4n+8}$ magic series are chiral with quasi-D_2 symmetry for the Au−S framework.[20,25] The cubic shape of the $Au_{36}(TBBT)_{24}$ nanocluster gives rise to higher symmetry (quasi-D_{2d} Au−S framework) than the other three nanoclusters, leading to an achiral structure.

The identical structure type (fcc) and the same surface-protecting ligand (TBBT) of this magic-series of nanoclusters permit a study of the periodicity of properties. The optical absorption spectra of the $Au_{8n+4}(TBBT)_{4n+8}$ nanoclusters exhibit similar profiles, featuring an intense ~400 nm peak in the UV region and a plateau in the longer visible wavelength region (Figure 3A). As the size increases from Au_{28}, Au_{36}, Au_{44}, to Au_{52}, the short-wavelength peak slightly redshifts from 366, 376, 380, to 396 nm, and the onset of the absorbance (e.g., optical gap) exhibits more redshifts from 702, 704, 820, to 890 nm (E_g = 1.77, 1.76, 1.51, 1.39 eV, respectively). The measured absorption coefficients (ε, M^{-1} cm^{-1}) of the four sizes are of the same magnitude, with 1.1×10^5 for Au_{28} at 366 nm, 2.0×10^5 for Au_{36} at 376 nm, 0.9×10^5 for Au_{44} at 380 nm, and 1.5×10^5 for Au_{52} at 396 nm. Such a similarity and uniform evolution in UV–vis profiles are in sharp contrast to the spectra of other discrete-sized gold nanoclusters with varied structures and surfaces.[7]

This magic series is akin to the well-defined quantum systems such as quantum dots and conjugated alkenes. The quantum confinement nature of the latter two has been well understood.[19] For example, the size-dependent HOMO–LUMO gaps of conjugated alkenes can be explained by solving the Schrödinger equation for a 1D "particle in a box". Intuitively, the $Au_{8n+4}(TBBT)_{4n+8}$ nanoclusters can be viewed as the three-dimensional (3D) quantum boxes, and their quantum confinement nature can be analyzed by a 3D "particle in a box" model, with the x, y directions of the box being fixed and the z direction being elongated. The electrons are confined in the small volume of the box (e.g., $0.6 \times 0.6 \times 0.2l$ nm^3, where l = 2−5 for the four sizes, respectively, Figure 2F) defined by the surface thiolate ligands. Based on such a quantum box model, the energy levels of the magic series can be calculated by the equation:

$$E = k\left(n_x^2 + n_y^2 + \frac{9}{l^2}n_z^2\right), \quad \text{where } k = \frac{h^2}{8m(0.2 \times 3 \times 10^{-9})^2}$$

The quantized energy levels are drawn in Figure S2, and only the 6s electrons of gold atoms in the central part (without bonding to any thiolate) are used to fill the energy levels (i.e., 2e, 4e, 6e, and 8e for the four sizes, Figure 2C). This gives rise to energy gaps $\Delta E = 3k$, $3k$, $1.5k$, $1.08k$ for the four sizes. This model partially explains the size-dependent trend and why the Au_{28} and Au_{36} have practically the same band gap.

We further performed real-time and real-space density functional theory (DFT) calculations[31] of the nanoclusters in order to provide a better correlation between their sizes and optical gaps. Figure 3B shows oscillator strengths of $Au_{8n+4}(TBBT)_{4n+8}$ nanoclusters. The onset of the optical absorption spectra redshifts from 1.72 to 1.34 eV as the cluster size increases from Au_{28} to Au_{52}, although the peak position for Au_{36}, 1.75 eV, is almost the same as that for Au_{28}. This computational result is well in accordance with the experimental one. To understand the origin of the peak shift, we plot the energies of HOMO−4 up to LUMO+4 of the magic series (Figure 3C). As the nanocluster size increases, the HOMO–LUMO energy gap decreases from 1.34 eV for Au_{28} to 1.25 eV for Au_{52}, except for $Au_{36}(TBBT)_{24}$. The HOMO–LUMO gap dependence on the cluster size is a manifestation of quantum confinement effect and has qualitatively the same tendency as the peak shift of the optical absorption spectra. Furthermore, the

DOI: 10.1021/jacs.5b12747
J. Am. Chem. Soc. 2016, 138, 3950–3953

distribution of the Kohn−Sham orbitals becomes dense near the HOMO and LUMO for the larger nanoclusters. These features of the orbitals cause significant enlargement of the oscillator strength at lower excitation energies and contribute to the red shift of the optical spectra. The ∼400 nm peak is mainly attributed to the d → sp transition and is less sensitive to size change than the long-wavelength peak arising from sp → sp transition in the kernel, since d electrons are less delocalized than the sp electrons.

Finally, it is worth exploring the empirical scaling relation of the band gap with the cluster size.[7] An $E_g \sim 1/L^2$ scaling law is found for the Au_{36}, Au_{44}, and Au_{52} (Figure 3D), where L is the length in the z direction of the cluster. This relation is consistent with the quantum confinement effect in the "particle in a box" model. Future work including more data points will be helpful to further examine the scaling relation.

In conclusion, we have demonstrated the existence of "periodicity" in the metal nanoclusters, as reflected in the uniform progression of magic numbers, the ordered growth patterns, and size-dependent quantum confinement effects in the $Au_{8n+4}(TBBT)_{4n+8}$ magic series. This magic series eliminates the complications by other variables (e.g., core structural types, surface ligand types) and thus simplifies the study of nanocluster properties and the periodicities in structural patterns, valence electron counts, and optical gaps. More magic series and periodicities may be discovered in future work.

■ ASSOCIATED CONTENT

Supporting Information

Experimental details and data. The Supporting Information is available free of charge on the ACS Publications website at DOI: 10.1021/jacs.5b12747.

■ AUTHOR INFORMATION

Corresponding Authors

*rongchao@andrew.cmu.edu

*nobusada@ims.ac.jp

Notes

The authors declare no competing financial interest.

■ ACKNOWLEDGMENTS

R.J. acknowledges support from the Air Force Office of Scientific Research under AFOSR award no. FA9550-15-1-9999 (FA9550-15-1-0154) and the Camille Dreyfus Teacher-Scholar Awards Program. K.N. acknowledges support from JSPS KAKENHI (No. 25288012) and ESICB. Computations were performed by the K computer (Nos. hp140054, 150218) and computer facilities at RCCS, Okazaki. We thank Dr. Zhongrui Zhou for ESI-MS analysis.

■ REFERENCES

(1) Qian, H.; Zhu, M.; Wu, Z.; Jin, R. *Acc. Chem. Res.* **2012**, *45*, 1470.

(2) Reveles, J. U.; Khanna, S. N.; Roach, P. J.; Castleman, A. W. *Proc. Natl. Acad. Sci. U. S. A.* **2006**, *103*, 18405.

(3) Wan, X.-K.; Tang, Q.; Yuan, S.-F.; Jiang, D.-e.; Wang, Q.-M. *J. Am. Chem. Soc.* **2015**, *137*, 652.

(4) Wang, Y.; Su, H.; Xu, C.; Li, G.; Gell, L.; Lin, S.; Tang, Z.; Häkkinen, H.; Zheng, N. *J. Am. Chem. Soc.* **2015**, *137*, 4324.

(5) Dhayal, R. S.; Liao, J. H.; Liu, Y. C.; Chiang, M. H.; Kahlal, S.; Saillard, J. Y.; Liu, C. *Angew. Chem., Int. Ed.* **2015**, *54*, 3702.

(6) AbdulHalim, L. G.; Bootharaju, M. S.; Tang, Q.; Del Gobbo, S.; AbdulHalim, R. G.; Eddaoudi, M.; Jiang, D. E.; Bakr, O. M. *J. Am. Chem. Soc.* **2015**, *137*, 11970.

(7) Jin, R. *Nanoscale* **2015**, *7*, 1549.

(8) (a) Zeng, C.; Chen, Y.; Das, A.; Jin, R. *J. Phys. Chem. Lett.* **2015**, *6*, 2976. (b) Chen, Y.; Zeng, C.; Kauffman, D. R.; Jin, R. *Nano Lett.* **2015**, *15*, 3603.

(9) Zeng, C.; Chen, Y.; Kirschbaum, K.; Appavoo, K.; Sfeir, M. Y.; Jin, R. *Sci. Adv.* **2015**, *1*, e1500045.

(10) Chen, Y.; Zeng, C.; Liu, C.; Kirschbaum, K.; Gayathri, C.; Gil, R. R.; Rosi, N. L.; Jin, R. *J. Am. Chem. Soc.* **2015**, *137*, 10076.

(11) Song, Y.; Fu, F.; Zhang, J.; Chai, J.; Kang, X.; Li, P.; Li, S.; Zhou, H.; Zhu, M. *Angew. Chem., Int. Ed.* **2015**, *54*, 8430.

(12) Crasto, D.; Barcaro, G.; Stener, M.; Sementa, L.; Fortunelli, A.; Dass, A. *J. Am. Chem. Soc.* **2014**, *136*, 14933.

(13) Pei, Y.; Zeng, X. C. *Nanoscale* **2012**, *4*, 4054.

(14) Cleveland, C. L.; Landman, U.; Schaaff, T. G.; Shafigullin, M. N.; Stephens, P. W.; Whetten, R. L. *Phys. Rev. Lett.* **1997**, *79*, 1873.

(15) Zhu, M.; Aikens, C. M.; Hollander, F. J.; Schatz, G. C.; Jin, R. *J. Am. Chem. Soc.* **2008**, *130*, 5883.

(16) (a) Ramakrishna, G.; Varnavski, O.; Kim, J.; Lee, D.; Goodson, T. *J. Am. Chem. Soc.* **2008**, *130*, 5032. (b) Varnavski, O.; Ramakrishna, G.; Kim, J.; Lee, D.; Goodson, T. *J. Am. Chem. Soc.* **2010**, *132*, 16. (c) Yau, S. H.; Varnavski, O.; Goodson, T. *Acc. Chem. Res.* **2013**, *46*, 1506.

(17) Negishi, Y.; Nakazaki, T.; Malola, S.; Takano, S.; Niihori, Y.; Kurashige, W.; Yamazoe, S.; Tsukuda, T.; Häkkinen, H. *J. Am. Chem. Soc.* **2015**, *137*, 1206.

(18) Konishi, K. Phosphine-Coordinated Pure-Gold Clusters: Diverse Geometrical Structures and Unique Optical Properties/Responses. In *Gold Clusters, Colloids and Nanoparticles I*; Mingos, D. M. P., Ed.; Springer: Berlin, 2014; Vol. *161*, pp 49−86.

(19) (a) Murray, C.; Norris, D. J.; Bawendi, M. G. *J. Am. Chem. Soc.* **1993**, *115*, 8706. (b) Alivisatos, A. P. *Science* **1996**, *271*, 933. (c) Atkins, P.; Paula, J. D. *Atkins' Physical Chemistry*, 8th ed., W. H. Freeman and Company: New York, 2006.

(20) (a) Zeng, C.; Li, T.; Das, A.; Rosi, N. L.; Jin, R. *J. Am. Chem. Soc.* **2013**, *135*, 10011. (b) Zeng, C.; Qian, H.; Li, T.; Li, G.; Rosi, N. L.; Yoon, B.; Barnett, R. N.; Whetten, R. L.; Landman, U.; Jin, R. *Angew. Chem., Int. Ed.* **2012**, *51*, 13114. (c) Zeng, C.; Chen, Y.; Liu, C.; Nobusada, K.; Rosi, N. L.; Jin, R. *Sci. Adv.* **2015**, *1*, e1500425.

(21) Jiang, D.-e. *Nanoscale* **2013**, *5*, 7149.

(22) Knoppe, S.; Malola, S.; Lehtovaara, L.; Bürgi, T.; Häkkinen, H. *J. Phys. Chem. A* **2013**, *117*, 10526.

(23) Pei, Y.; Lin, S.; Su, J.; Liu, C. *J. Am. Chem. Soc.* **2013**, *135*, 19060.

(24) (a) Chevrier, D. M.; Chatt, A.; Zhang, P.; Zeng, C.; Jin, R. *J. Phys. Chem. Lett.* **2013**, *4*, 3186. (b) Chevrier, D. M.; Zeng, C.; Jin, R.; Chatt, A.; Zhang, P. *J. Phys. Chem. C* **2015**, *119*, 1217.

(25) Zeng, C.; Chen, Y.; Li, G.; Jin, R. *Chem. Commun.* **2014**, *50*, 55.

(26) Xu, W. W.; Li, Y.; Gao, Y.; Zeng, X. C. *Nanoscale* **2016**, *8*, 1299.

(27) (a) Teo, B. K.; Zhang, H. *Proc. Natl. Acad. Sci. U. S. A.* **1991**, *88*, 5067. (b) Mednikov, E. G.; Dahl, L. F. *J. Am. Chem. Soc.* **2008**, *130*, 14813. (c) Mednikov, E. G.; Ivanov, S. A.; Dahl, L. F. *Angew. Chem., Int. Ed.* **2003**, *42*, 323.

(28) (a) Takahata, R.; Yamazoe, S.; Koyasu, K.; Tsukuda, T. *J. Am. Chem. Soc.* **2014**, *136*, 8489. (b) Takano, S.; Yamazoe, S.; Koyasu, K.; Tsukuda, T. *J. Am. Chem. Soc.* **2015**, *137*, 7027.

(29) Zeng, C.; Liu, C.; Chen, Y.; Rosi, N. L.; Jin, R. *J. Am. Chem. Soc.* **2014**, *136*, 11922.

(30) Wiseman, M. R.; Marsh, P. A.; Bishop, P. T.; Brisdon, B. J.; Mahon, M. F. *J. Am. Chem. Soc.* **2000**, *122*, 12598.

(31) (a) Iida, K.; Noda, M.; Ishimura, K.; Nobusada, K. *J. Phys. Chem. A* **2014**, *118*, 11317. (b) Noda, M.; Ishimura, K.; Nobusada, K.; Yabana, K.; Boku, T. *J. Comput. Phys.* **2014**, *265*, 145.

DOI: 10.1021/jacs.5b12747
J. Am. Chem. Soc. 2016, 138, 3950−3953